Realization of Metal−Insulator Transition and Oxidation in Silver Nanowire Percolating Networks by Terahertz Reflection Spectroscopy

Yao-Jiun Tsai, Chi-Ying Chang, Yi-Chun Lai, Pei-Chen Yu, and Hyeyoung Ahn*

Department of Photonics and Institute of Electro-Optical Engineering, National Chiao-Tung University, Hsinchu 30010, Taiwan, Republic of China

S Supporting Information

ABSTRACT: Metal nanowires (NWs) enable versatile applications in printed electronics and optoelectronics by serving as thin and flexible transparent electrodes. The performance of metal NWs as thin electrodes is highly correlated to the connectivity of NW meshes. The percolation threshold of metal NW films corresponds to the minimum density of NWs to form the transparent, yet conductive metal NW networks. Here, we determine the percolation threshold of silver NW (AgNW) networks by using morphological analysis and terahertz (THz) reflection spectroscopy. From the divergent behavior of carrier scattering time and the increase of carrier backscattering factor, the critical NW density at which crossover from Drude to non-Drude behavior of THz conductivity occurs can be unambiguously determined for AgNW thin films. Furthermore, the natural oxidation of AgNWs which causes the gradual reduction of the connectivity of the AgNW network is also realized by the THz spectroscopy. The selective oxidation of NW-to-NW junctions weakens the ohmic contact, and for AgNWs near a critical density, it can even lead to metal−insulator transition. The presented results offer invaluable information to accelerate the deployment of metal nanowires for next-generation electronics and optoelectronics on flexible substrates.

KEYWORDS: transparent electrode, silver nanowires, terahertz spectroscopy, oxidation, percolation transition, non-Drude model
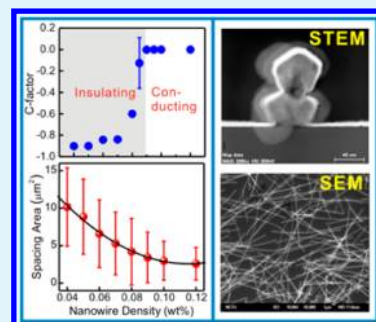
Highly transparent but still conducting electrode films are crucial for many optoelectronic devices including flat panel or plasma displays and solar cells. Indium-tin-oxide (ITO) is the most widely used transparent conducting metal oxide for this purpose. However, its poor physical properties make ITO unlikely to be the material of flexible optoelectronic devices, and the cost of sputtered ITO is too high to produce large area devices.[1] In addition, the high-temperature sputtering deposition of ITO can cause damage on the organic active layers in solar cells and display devices. Conducting polymers,[2,3] nanoparticle metal oxides,[4] carbon nanotubes,[5−7] and graphene[8−10] have been investigated as potential alternatives to ITO. Recently, nanostructured thin metal films emerge as a promising material to replace ITO. For example, Ag nanowire (AgNW) thin film can be spin-coated or spray-casted over nearly any substrate at room temperature and shows the potential for realization of cheap, flexible, and transparent electrodes.[11−17] In the AgNW thin film, NWs collectively behave as a random metal network with high transparency, but as the concentration of NWs (D) increases, there is a trade-off between transparency and conductivity, and it is necessary to find the proper conditions for AgNW films to keep both high transparency and high conductivity. In particular, the conductivity of AgNW films is closely related with the long-range connectivity of NWs, which can be realized by the percolation threshold. The AgNW films with super-percolation network have high electrical conductivities, which are attributed to the increase of NW-to-NW contact junctions and the long diffusion length of carriers through the NW metal network.

While the optical properties of materials can be characterized by conventional ellipsometry or reflectometry techniques, the electrical properties are difficult to investigate through the intensity-sensitive measurement techniques. The electrical conductivity of materials is typically determined by the direct contact of the conductive probe on the samples, but for nanostructured materials, it can be a challenge to fabricate direct ohmic contact on nanostructures. Recently, terahertz (THz) spectroscopy has been extensively used to characterize the electrical conductivities of various materials, ranging from semiconductors to biomolecules. Since THz time-domain spectroscopy (THz-TDS) is an optical and noncontact method, it can also easily be integrated with various types of nanostructures to characterize their dielectric and transport properties.

For thin conductive films, the frequency dependence of conductivity $\sigma(\omega)$ shows simple Drude behavior. For nanostructures, however, carriers are confined within the individual or semi-connected nanostructures, and $\sigma(\omega)$ deviates
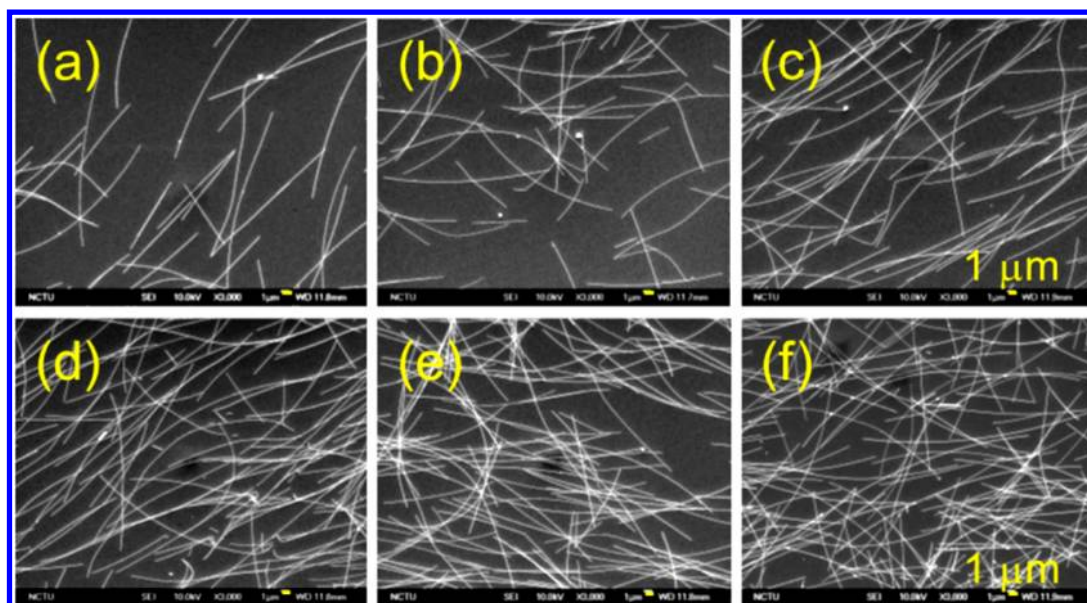
Figure 1. (a−f) SEM images of AgNW thin films with concentrations of 0.04, 0.06, 0.08, 0.09, 0.10, and 0.12 wt %, respectively. It is clearly seen that AgNWs in (d−f) form a metal network covering the whole sample area, while those in (a−c) form a partially connected network.
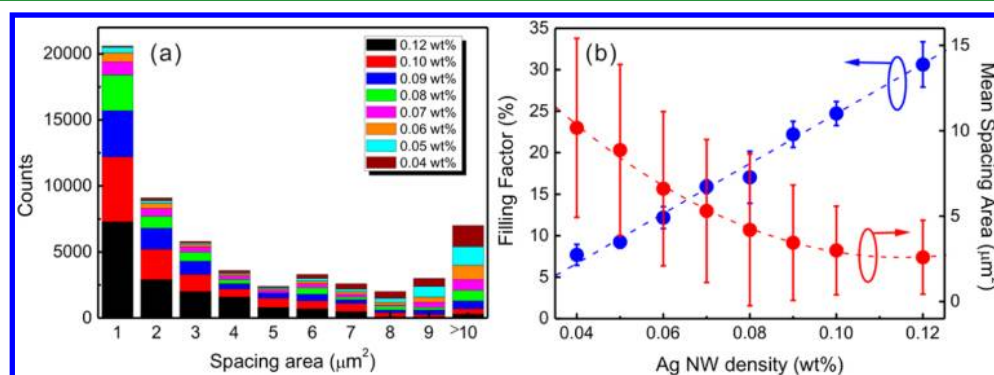

Figure 2. Morphological analysis of AgNW thin films, including a histogram of the spacing area distribution (a) and the areal filling factor and spacing areas as a function of AgNW concentration (b). The spacing areas calculated for each AgNW film are shown in Figure S3 (Supporting Information).

from the Drude behavior. Recently, non-Drude THz conductivities in various nanomaterials have been successfully described by the Drude−Smith model,[18] which takes account of the scattering, especially backscattering, events of electrons due to the localization within the nanostructures. For disconnected three-dimensional nanostructure assembly, such as vertically grown nanorods, conduction electrons are localized within the individual nanostructures, and the backscattering event can be significant as the size of the nanostructure decreases. Meanwhile, for randomly connected two-dimensional NW films, electrons transport through the NW-to-NW junctions, and the backscattering event due to the localization can be reduced as the NW density increases. With further increase of NW density above a critical value, the NW network undergoes a transition from insulating to conducting phase, and accordingly, the electrical conductivity shows the crossover from non-Drude-like to Drude-like behavior. In this work, by using the THz-TDS system, we systematically investigated the electrical conductivity of AgNW thin films prepared with a wide range of NW concentrations. By investigating the electrical properties of the two-dimensional AgNW network near the metal−insulator transition, we could determine the minimum NW

density (D_c), required to show the highest optical transmittance and yet conducting behavior.

■ RESULTS AND DISCUSSION

Before measuring the THz conductivity, we evaluated the optical transparency related to the morphological properties of AgNWs. The distribution of AgNWs with various concentrations and the formation of the NW network were investigated by field emission scanning electron microscopy (FE-SEM). The SEM images in Figure 1(a)−(f) show that AgNWs are randomly oriented without preferential direction and significant bundling of wires over the area of the substrate, allowing the use of percolation theory to describe the AgNW networks. For quantitative analysis of the AgNW network, the distribution histograms of spacing areas enclosed by NWs and the areal filling factors are calculated from the SEM images and plotted as a function of NW density in Figure 2. The areal filling factor in Figure 2(b) is the average projected area of NWs and is proportional to the NW density. The optical transmittance spectra of AgNW samples are measured in the spectral range of 400−2000 nm and illustrated in Figure S1 (Supporting Information). The optical transmittance decreases
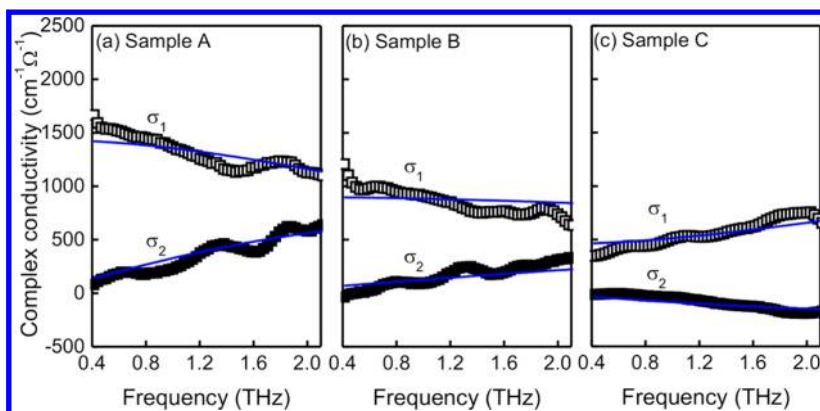
Figure 3. (a−c) Frequency dependence of complex conductivity of AgNW thin films, samples A, B, and C, respectively, calculated from the THz reflectance data. The solid lines in (a) and (b) are obtained by using the Drude model and that in (c) by using the Drude−Smith model.

with the increase of NW density, but it is still higher than 90% even for a NW film of the highest NW density. Since the optical transmittance of AgNW films is due to the reflective light scattering by AgNWs, the increase of areal filling factor can cause the loss in the optical transmittance, and their linear relation is shown in Figure S2 (Supporting Information).

Meanwhile, it is noteworthy that the spacing areas enclosed by AgNWs in Figure 2(b) show a percolation-like dependence on NW density. According to the percolation theory, the conductivity scales as $\sigma \propto (D - D_c)^\alpha$ for $D > D_c$, where the critical exponent, α, depends on the dimensionality of space.[19] Since the spacing area is the open area enclosed by the NWs, it elucidates the appearance of a complete loop of the conducting network and may be directly related to the conductivity of the AgNW network. By using the typical percolation expression, we fitted the NW density dependence of the spacing area and obtained the percolation threshold NW density of ∼0.105 wt % and the percolation dimension of 1.44 ± 0.08, which is close to what the percolation theory predicts for two-dimensional films, 1.33.[20]

To demonstrate the detailed analysis of the THz spectroscopy, we selected three samples (A, B, and C) with the concentrations of 0.12, 0.10, and 0.08 wt %, and the following THz analyses are given only for these three samples. The complex refractive index ($\tilde{n} = n + i\kappa$) and the electrical conductivity ($\tilde{\sigma}(\omega) = \sigma_1 + i\sigma_2$) of samples are obtained by analyzing the specularly reflected THz spectra from AgNW films. For samples A and B, the complex conductivities in Figure 3(a) and 3(b) show the typical Drude behavior below the plasma frequency, indicating that NWs in these films form a conductive metal network. By using the simple Drude model, we obtained the plasma frequency ω_p ($= (Ne^2/m^*\varepsilon_0)^{1/2}$) and the carrier scattering time τ_0, where the electron effective mass (m^*) of the AgNW is assumed to be $0.868m_0$.[21]

Meanwhile, the real part of the conductivity σ_1 for sample C, shown in Figure 3(c), gradually increases, whereas σ_2 with a negative value decreases as the frequency increases. This $\sigma(\omega)$ cannot be explained by the simple Drude model. The complex conductivity of sample C is then fitted by using the Drude−Smith model. In the Drude−Smith model, the complex conductivity is given by[16]

$$\sigma(\omega) = \frac{\varepsilon_0\omega_p^2\tau_0}{1 - i\omega\tau_0}\left[1 + \frac{c}{(1 - i\omega\tau_0)}\right] \quad (1)$$

where c is a parameter describing the fraction of the electron's original velocity after some number of scattering events and varies between −1 and 0, corresponding to Drude conductivity for $c = 0$ and complete backscattering for $c = -1$. A negative value of c reflects that the confined electrons within the individual NWs may experience a preferential backward scattering. The solid lines in Figure 3(c) were obtained with $c = -0.6$, indicating that a large portion of electrons are confined within the individual NWs and cannot transport through the NW junctions because of the low connectivity between the NWs. The fitting parameters as well as the statistical parameters for three samples are given in Table 1.

Table 1. Statistical Parameters and the Best Fit Parameters for Samples A, B, and C[a]

sample	AgNW density (wt %)	spacing area (μm^2)	$\omega_p/2\pi$ (THz)	τ_0 (fs)	c
A	0.12	2.6	546	39	0
B	0.10	3.0	573	30	0
C	0.08	4.2	818	24	−0.6

[a]The spacing areas are taken from Figure 2(b), and $\omega_p/2\pi$ and τ_0 for each sample are estimated from the fitting process of complex conductivity with either the Drude or Drude−Smith model.

The same analysis was applied to a series of AgNW films grown with different NW densities. From the fits to the measured $\sigma_1(\omega)$ and $\sigma_2(\omega)$, a set of fitting parameters ω_p, τ_0, and c were obtained for each sample, and their dependence on the NW density is summarized in Figure 4. Noticeably, the c value changes from 0 to a nonzero, negative value near a critical density $D_c \sim 0.090 \pm 0.005$ wt %. This transitional change of c-values at the critical density indicates that there is the crossover from the conducting to insulating phase in the AgNW network. Furthermore, the scattering time τ_0 abruptly increases only near D_c but is otherwise nearly concentration-independent. Similar divergence-like behavior of τ_0 was observed for nanometer-thick gold films,[22] and this behavior was suggested to be related to the discontinuity in dielectric constant of system at the threshold of metal-insulating percolation transition.[23] The critical density $D_c \sim 0.09$ wt % is comparable to the percolation threshold density of 0.105 wt % obtained from the morphological analysis above. The large error bar in Figure 4(a) for samples with $D \sim D_c$ is due to the nearly flat responses of σ_1 and σ_2 as shown in the inset.
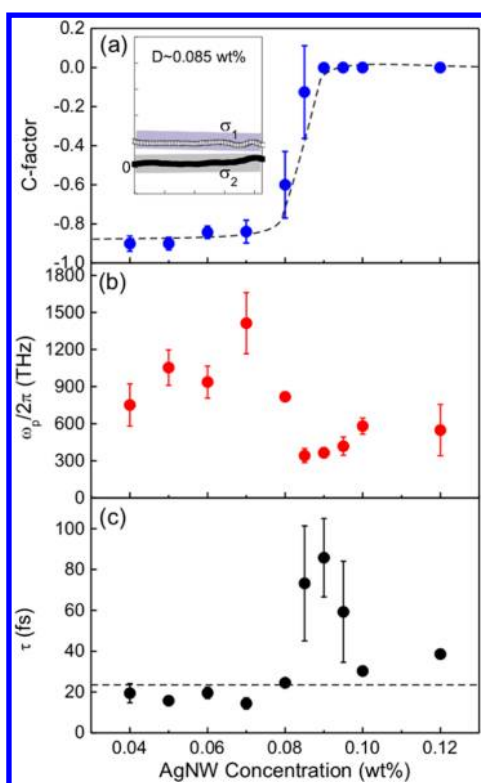
Figure 4. AgNW concentration dependence of the best-fit parameters. Below the critical AgNW concentration $D_c \sim 0.09$ wt %, the fitting parameters are obtained by using the Drude−Smith model, while above D_c, the parameters are obtained by using the Drude model. The divergent behavior of τ near D_c indicates the metal−insulator transition near the percolation threshold. Dashed line in (a) is drawn as a guide for the eye. (Inset) THz conductivity for a sample with $D \sim 0.085$ wt %.

THz conductivity spectra also provide information on the local transport of carriers through the NW network. The charge transport through NWs includes two components: along the wires and across the junctions. For AgNWs, it is known that the reduction of the junction resistance is crucial in the determination of conductive properties of the AgNW electrode. Several methods have been proposed to reduce the junction resistance, including plasmonic welding of the NW film[24] and Au coating on NWs.[13] Meanwhile, oxidation of AgNW surfaces may increase the junction resistance and hamper the performance of AgNW-based devices. Particularly, NWs with large surface area can be easily affected by either natural or enforced oxidation. Therefore, the characterization of oxidation and its influence on the conductivity of NWs are of importance in the long-term performance of devices based on metal nanostructures.

For the investigation of the influence of the oxidation on the electrical property of AgNW film, another AgNW film (sample D) with $D \sim D_c$ was prepared. Figure 5 shows the complex electrical conductivity of sample D measured within a day after the growth of AgNW film ($\sigma_{1\text{-day}}$) and after being stored for one month in air ($\sigma_{1\text{-month}}^{air}$), respectively. Obviously, $\sigma_{1\text{-day}}(\omega)$ can be described by the Drude model, but after the exposure to air for one month, $(\sigma_{1\text{-month}}^{air})(\omega)$ shows non-Drude behavior. We believe the transition from the conducting to the insulating phase is attributed to the growth of thin naturally oxidized layers on AgNW surfaces. Oxidation at the NW junctions can lead to the non-ohmic contact between NWs and break apart
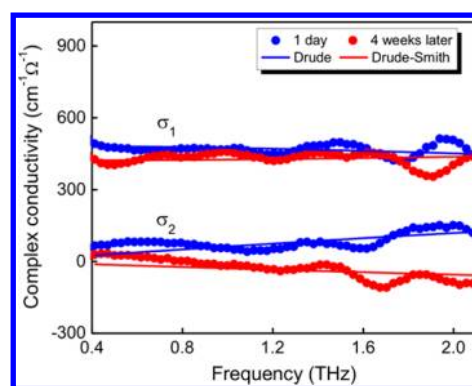

Figure 5. Electrical conductivities of sample D measured within a day after the deposition (blue) and after one month being stored in air (red), respectively. The solid lines are obtained by applying the Drude and the Drude−Smith model to $\sigma_{1\text{-day}}$ and $\sigma_{1\text{-month}}^{air}$, respectively.

the NW network. A decrease of electrical conductivity due to the natural oxidation of AgNWs is consistent with the previously reported result of the increase of sheet resistance for thermally oxidized AgNWs.[25]

To provide the metal composition analysis of NWs, $\omega−2\theta$ X-ray diffraction (XRD) curves were measured for sample D before and after oxidation. Narrow Ag(220) peaks in Figure 6
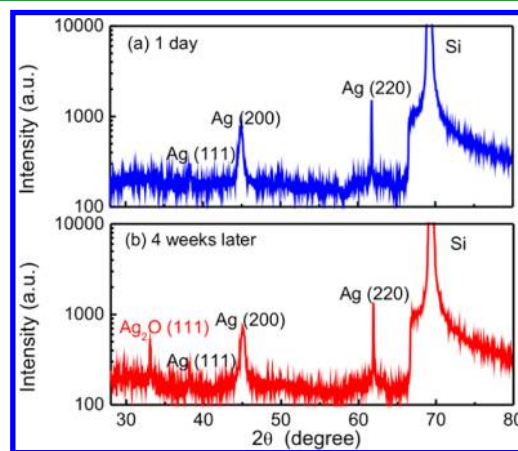

Figure 6. X-ray diffraction curves for sample D measured (a) within a day after the deposition of AgNW film and (b) after being stored for one month in air, respectively. Besides peaks for Ag(111), (200), and (220), a peak corresponding to $Ag_2O(111)$ was observed in (b), demonstrating that naturally oxidized layers are formed on the surfaces of AgNWs.

show that our AgNWs are single-crystalline wires with a preferred orientation along the long wire axis in the [110] direction, as widely reported about Ag nanowires.[26,27] In Figure 6(b), a peak corresponding to $Ag_2O(111)$ is observed at about 33° for the oxidized sample D, which is absent for as-prepared sample D in Figure 6(a). A small decrease of the peak values at both Ag(100) and Ag(110) in Figure 6(b) compared to those in Figure 6(a) indicates that the oxidation occurs only at the surface of the AgNWs.

Additional compositional analyses for Ag and O atoms are performed by using scanning transmission electron microscopy (STEM). Figure 7(a) and 7(d) illustrate the cross-sectional STEM images of a single pentagonal AgNW and the stacked AgNWs, respectively, in the oxidized sample D. Apparently, the contact surfaces between the AgNW and Si substrate in Figure
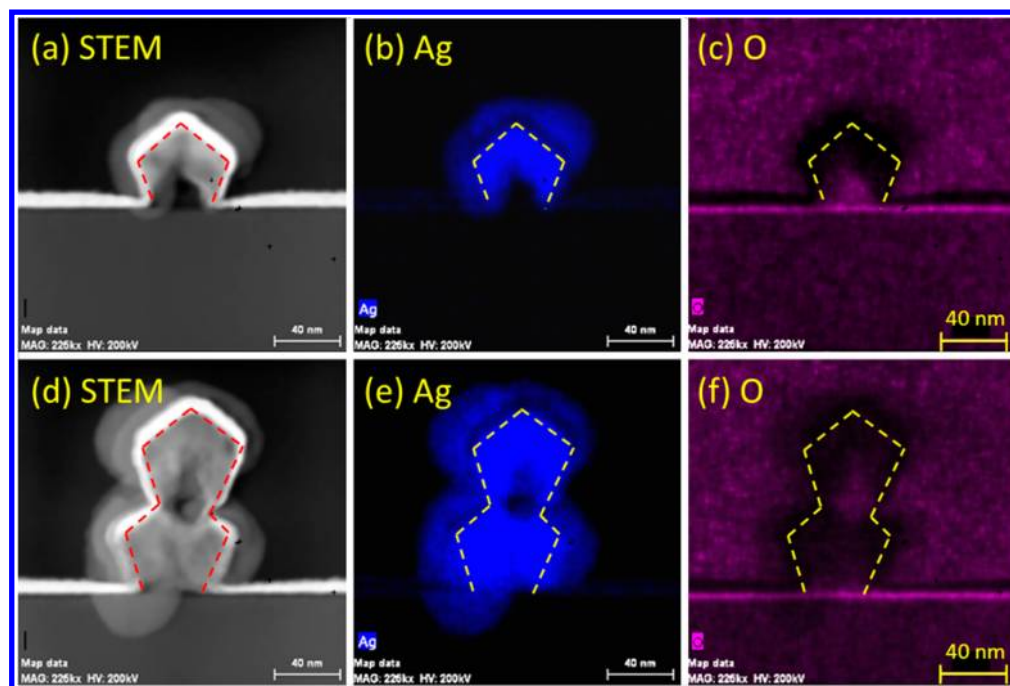
633

dx.doi.org/10.1021/am404717j | ACS Appl. Mater. Interfaces 2014, 6, 630−635

Figure 7. Cross-sectional STEM and EDS mapping images of oxidized sample D. (a–d) STEM images of a single AgNW and stacked AgNWs, respectively. EDS mapping images in (b) and (e) correspond to Ag atoms and those in (c) and (f) for O atoms. Dashed lines are guides for the eyes of pentagonal AgNWs.

7(a) and between two AgNWs in Figure 7(b) appear darker than other NW areas, and we used the energy-dispersive X-ray spectroscopy (EDS) to analyze their compositions. In EDS, characteristic X-rays are caused by inelastic scattering of electrons as they pass through the sample during the STEM measurement. X-ray signals provide a unique signature to identify the type of atoms present, and the content of the element can be analyzed from the intensity of the peak. The EDS mappings in Figure 7(b) and 7(e) correspond to the characteristic X-rays emitted by Ag atoms, while those in Figure 7(c) and 7(f) correspond to the X-rays by O atoms present in a single NW and the stacked NWs, respectively. For both a single NW and the stacked NWs, weak, but clear, X-ray signals by oxygen atoms are observed, implying the oxidation of AgNWs in sample D. Of particular interest observed in Figure 7 is that the major oxidation occurs at the surface of contact with the substrate or at the NW-to-NW junction. This local oxidation shows a sharp contrast to the oxidation of other metal or semiconductor nanostructures, such as Si NWs with shell-like SiO_2 layer grown on the surface around the core Si.[28] The local oxidation of AgNWs might be due to the accelerated oxidation occurring at the interface of contact, and it would be interesting to characterize the oxidation process of AgNWs in more detail; however, that is beyond the scope of this paper. Upon the basis of the above analyses, it can be concluded that natural oxidation of AgNWs can lead to the non-ohmic contact at the NW junctions and significantly reduce the conductivity of AgNW films.

CONCLUSIONS

In conclusion, we have performed the THz spectroscopic measurement on thin AgNW films, which can provide new information and insights about the electrical characteristics of the AgNW film. Highly transparent (>90%) and electrically conductive AgNW films are realized when the NW density is

above a critical value. Below the critical density, the electrical conductivity shows the non-Drude behavior, and its frequency dependence, especially the negative values of the imaginary part of conductivity, can be described by the Drude–Smith model. The divergence of the scattering time and the onset of nonzero c values near the critical density correspond to the metal–insulator percolation transition. In cooperation with morphological analyses, THz spectroscopy also successfully elucidates the natural oxidation of AgNWs. The oxidized NW junctions developed during the exposure to air prevent the charged carriers from transporting through the NW junctions and considerably reduce the conductivity of AgNW networks. Finally, this work points to the advantages of THz spectroscopy for a full quantitative analysis of the metal nanostructure network.

EXPERIMENTAL SECTION

Preparation of AgNW Film. For this study, we prepared eight AgNW films with different concentrations varied from 0.04 to 0.12 wt % by using a spin-coating method on Si substrates. Commercially available AgNWs with average lengths/diameters of 10 μm/70–100 nm were stored in isopropyl alcohol solvent and subsequently diluted to a proper concentration by the same solvent. A micropipet was used to drop AgNW suspension on the Si substrates and then spun-cast at 1200 rpm for 40 s. For natural oxidation measurement, several selected samples were stored in a desiccator cabinet without flowing nitrogen gas to maintain a clean and humidity-controlled environment.

Characterization System. The morphology and the distribution of AgNWs across the substrate were analyzed by using field-emission scanning electron microscopy (FE-SEM). From the same magnification-frame SEM images, the areal filling factor, the area covered by AgNWs, and the spacing area enclosed by NW meshes were calculated for AgNW films with various concentrations. Optical transmittance was measured using a dual light source and integrating sphere system. A barium sulfate coated integrating sphere with a diameter of 6 cm was used to collect the total transmitted light. The electrical conductivities of AgNW films were measured by the THz-TDS technique. Our

home-made THz-TDS system is based on THz emission from a photoconductive antenna and free-space electro-optic sampling detection. The excitation of the emitter and the probe of THz signal were achieved by a Ti:sapphire laser which delivers ~150 fs optical pulses at a center wavelength of 800 nm. Since the THz transmittance of NW samples decreases significantly with the increase of NW concentration (especially for $D > D_c$), we measured specularly reflected THz signals from the AgNW films at 45° to elucidate the electrical properties of AgNW films. A gold-coated mirror was used as a reference material for the reflectance measurement.

ASSOCIATED CONTENT

Ⓢ Supporting Information

The statistical results of spacing areas enclosed by AgNWs and optical transmittance spectra for AgNWs with various concentrations. This material is available free of charge via the Internet at http://pubs.acs.org.

AUTHOR INFORMATION

Corresponding Author

*Tel.: +886-3-5712121. Fax: +886-3-5716631. E-mail: hyahn@mail.nctu.edu.tw.

Notes

The authors declare no competing financial interest.

ACKNOWLEDGMENTS

ABBREVIATIONS

AgNW, silver nanowire; THz, terahertz; ITO, indium-tin-oxide; THz-TDS, THz time-domain spectroscopy; FE-SEM, field-emission scanning electron microscopy; XRD, X-ray diffraction; STEM, scanning transmission electron microscopy; EDS, energy-dispersive X-ray spectroscopy

REFERENCES

(1) Forrest, S. R. *Nature (London, U.K.)* **2004**, *428*, 911−918.

(2) Huang, J.; Wang, X.; deMello, A. J.; deMello, J. C.; Bradley, D. D. C. *J. Mater. Chem.* **2007**, *17*, 3551−3554.

(3) Na, S.-I.; Kim, S.-S.; Jo, J.; Kim, D.-Y. *Adv. Mater. (Weinheim, Ger.)* **2008**, *20*, 4061−4067.

(4) Yodyingyong, S.; Zhang, Q.; Park, K.; Dandeneau, C. S.; Zhou, X.; Triampo, D.; Cao, G. *Appl. Phys. Lett.* **2010**, *96*, 073115.

(5) Doherty, E. M.; De, S.; Lyons, P. E.; Shmeliov, A.; Nirmalraj, P. N.; Scardaci, V.; Joimel, J.; Blau, W. J.; Boland, J. J.; Coleman, J. N. *Carbon* **2009**, *47*, 2466−2473.

(6) Leem, D. S.; Kim, S.; Kim, J. W.; Sohn, J. I.; Edwards, A.; Huang, J. S.; Wang, X. H.; Kim, J. J.; Bradley, D. D. C.; deMello, J. C. *Small* **2010**, *6*, 2530−2534.

(7) Kim, S.; Yim, J.; Wang, X.; Bradley, D. D. C.; Lee, S.; de Mello, J. C. *Adv. Funct. Mater.* **2010**, *20*, 2310−2316.

(8) Kim, K. S.; Zhao, Y.; Jang, H.; Lee, S. Y.; Kim, J. M.; Ahn, J. H.; Kim, P.; Choi, J. Y.; Hong, B. H. *Nature (London, U.K.)* **2009**, *457*, 706−710.

(9) Eda, G.; Chhowalla, M. *Adv. Mater. (Weinheim, Ger.)* **2010**, *22*, 2392−2415.

(10) Wöbkenberg, P. H.; Eda, G.; Leem, D. S.; de Mello, J. C.; Bradley, D. D. C.; Chhowalla, M.; Anthopoulos, T. D. *Adv. Mater. (Weinheim, Ger.)* **2011**, *23*, 1558−1562.

(11) Sun, Y.; Xia, Y. *Adv. Mater. (Weinheim, Ger.)* **2002**, *14*, 833−837.

(12) Lee, J.-Y.; Connor, S. T.; Cui, Y.; Peumans, P. *Nano Lett.* **2008**, *8*, 689−692.

(13) De, S.; Higgins, T. M.; Lyons, P. E.; Doherty, E. M.; Nirmalraj, P. N.; Blau, W. J.; Boland, J. J.; Coleman, J. N. *ACS Nano* **2009**, *3*, 1767−1774.

(14) Hu, L.; Kim, H. S.; Lee, J.-Y.; Peumans, P.; Cui, Y. *ACS Nano* **2010**, *4*, 2955−2963.

(15) Zhu, R.; Chung, C.-H.; Cha, K. C.; Yang, W.; Zheng, Y. B.; Zhou, H.; Song, T.-B.; Chen, C.-C.; Weiss, P. S.; Li, G.; Yang, Y. *ACS Nano* **2011**, *5*, 9877−9882.

(16) Leem, D. S.; Edwards, A.; Faist, M.; Nelson, J.; Bradley, D. C.; deMello, J. C. *Adv. Mater. (Weinheim, Ger.)* **2011**, *23*, 4371−4375.

(17) Chung, C.-H.; Song, T.-B.; Bob, B.; Zui, R.; Yang, Y. *Nano Res.* **2012**, *5*, 805−814.

(18) Smith, N.V. *Phys. Rev. B: Condens. Matter Mater. Phys.* **2001**, *64*, 155106−4.

(19) Hu, L.; Hecht, D. S.; Gruner, G. *Nano Lett.* **2004**, *4*, 2513−2517.

(20) Stauffer, G. *Introduction to Percolation Theory*; Taylor & Francis: London, 1985.

(21) Kim, J.; Maeng, I.; Jung, J.; Song, H.; Son, J.-H.; Kim, K.; Lee, J.; Kim, C.-H.; Chae, G.; Jun, M.; Hwang, Y.; Lee, S. J.; Myoung, J.-M.; Choi, H. *Appl. Phys. Lett.* **2013**, *102*, 011109−4.

(22) Wakther, M.; Cooke, D. G.; Sherstan, C.; Hajar, M.; Freeman, M. R.; Hegmann, F. A. *Phys. Rev. B: Condens. Matter Mater. Phys.* **2007**, *76*, 125408−9.

(23) Grannan, D. M.; Garland, J. C.; Tanner, D. B. *Phys. Rev. Lett.* **1981**, *46*, 375−379.

(24) Garnett, E. C.; Cai, W.; Cha, J. J.; Mahmood, F.; Connor, S. T.; Christoforo1, M. G.; Cui, Y.; McGehee, M. D.; Brongersma, M. L. *Nat. Mater.* **2012**, *11*, 241−249.

(25) Ahn, Y.; Jeong, Y.; Lee, Y. *ACS Appl. Mater. Interfaces* **2012**, *4*, 6410−6414.

(26) Ni, C.; Hassan, P. A.; Kaler, E. W. *Langmuir* **2005**, *21*, 3334−3337.

(27) Hofmeister, H.; Nepijko, S. A.; Ievlev, D. N.; Schulze, W.; Ertl, G. *J. Cryst. Growth* **2002**, *234*, 773−781.

(28) Shir, D.; Liu, B. Z.; Mohammad, A. M.; Lew, K. K.; Mohney, S. E. *J. Vac. Sci. Technol. B* **2006**, *24*, 1333−1336.

635

dx.doi.org/10.1021/am404717j | *ACS Appl. Mater. Interfaces* 2014, 6, 630−635